REPORT DOCUMENTATION PAGE

Form Approved
OMB No. 0704-0188

1. AGENCY USE ONLY *(Leave blank)*	2. REPORT DATE	3. REPORT TYPE AND DATES COVERED
	August 1995	Professional Paper

4. TITLE AND SUBTITLE

STOCHASTIC DETERMINATION OF OPTIMAL WAVELET COMPRESSION STRATEGIES

5. FUNDING NUMBERS

PR: ZW67
PE: 0601152N
WU: DN303002

6. AUTHOR(S)

D. E. Waagen, J. D. Argast, and J. R. McDonnell

7. PERFORMING ORGANIZATION NAME(S) AND ADDRESS(ES)

Naval Command, Control and Ocean Surveillance Center (NCCOSC)
RDT&E Division
San Diego, CA 92152–5001

8. PERFORMING ORGANIZATION REPORT NUMBER

9. SPONSORING/MONITORING AGENCY NAME(S) AND ADDRESS(ES)

Office of Chief of Naval Research
Independent Research Program (IR)
Arlington, VA 22217–5000

10. SPONSORING/MONITORING AGENCY REPORT NUMBER

11. SUPPLEMENTARY NOTES

12a. DISTRIBUTION/AVAILABILITY STATEMENT

Approved for public release; distribution is unlimited.

12b. DISTRIBUTION CODE

13. ABSTRACT *(Maximum 200 words)*

Wavelet theory provides an attractive approach to signal and image compression. This work investigates a new approach for wavelet transform coefficient selection for efficient image compression. For a desired image compression ratio (50:1), wavelet scale thresholds are derived via a multiagent stochastic optimization process. Previous work has demonstrated an interscale relationship between the stochastically optimized wavelet coefficient thresholds. Based on the experimental results, a deterministic wavelet coefficient selection criterion is hypothesized and the constants of the equation statistically derived. Experimental results of the stochastic optimization and deterministic approaches are compared and contrasted with results from previously published wavelet coefficient threshold strategies.

Published in *Proceedings of SPIE Visual Communication Image Processing (VCIP)*, Vol. 2308, pp. 1711–1722, September 1994.

14. SUBJECT TERMS

Wavelet Transform
Image Compression
Stochastic Optimization

15. NUMBER OF PAGES

16. PRICE CODE

17. SECURITY CLASSIFICATION OF REPORT	18. SECURITY CLASSIFICATION OF THIS PAGE	19. SECURITY CLASSIFICATION OF ABSTRACT	20. LIMITATION OF ABSTRACT
UNCLASSIFIED	UNCLASSIFIED	UNCLASSIFIED	SAME AS REPORT

21a. NAME OF RESPONSIBLE INDIVIDUAL	21b. TELEPHONE *(include Area Code)*	21c. OFFICE SYMBOL
J. R. McDonnell	(619) 553–5762	Code 785

SPIE VCIP, SEP 1994

Stochastic determination of optimal wavelet compression strategies

D. E. Waagen, J. D. Argast,† and J. R. McDonnell‡

TRW Systems Integration Group, Ogden, UT 84403
†Aldus Corporation, Seattle, WA 98104
‡NCCOSC RDT&E Division, San Diego, CA 92152

ABSTRACT

Wavelet theory provides an attractive approach to signal and image compression. This work investigates a new approach for wavelet transform coefficient selection for efficient image compression. For a desired image compression ratio (50:1), wavelet scale thresholds are derived via a multiagent stochastic optimization process. Previous work has demonstrated an interscale relationship between the stochastically optimized wavelet coefficient thresholds. Based on the experimental results, a deterministic wavelet coefficient selection criterion is hypothesized and the constants of the equation statistically derived. Experimental results of the stochastic optimization and deterministic approaches are compared and contrasted with results from previously published wavelet coefficient threshold strategies.

Keywords: wavelet transform, image compression, stochastic optimization.

1. INTRODUCTION

Wavelets originated from the analysis of seismic data by J. Morlet.[1] A wavelet is a function ψ whose dilations and translations

$$\psi_{a,b}(t) = \frac{1}{\sqrt{a}} \psi\left(\frac{t-b}{a}\right), \quad a > 0, \quad b \in \Re \tag{1}$$

form a basis in L^2.[2,3] The continuous wavelet transform maps a function f to a set of wavelet coefficients which vary continuously over (a,b)

$$F(a,b) = \frac{1}{\sqrt{a}} \int f(t) \cdot \psi\left(\frac{t-b}{a}\right) dt. \tag{2}$$

Given an orthonormal wavelet basis, any L^2 function f can be represented as a (possibly infinite) summation

$$f(t) = \sum_{a,b} d_{a,b} \psi_{a,b}(t) \tag{3}$$

where the wavelet coefficients $d_{a,b}$ are defined as the scalar inner product

$$d_{a,b} = \int_{-\infty}^{\infty} f(t) \psi_{a,b}(t) dt. \tag{4}$$

The wavelet coefficients correspond to the projection of $f(t)$ onto the coefficient's associated wavelet. Wavelet basis sets can be orthogonal or non-orthogonal, and each wavelet can have compact or infinite support. For image compression, one does not want to transform the image into more coefficients than necessary to completely characterize the image. Orthogonal wavelets, such as the Haar and Daubechies wavelets, provide an efficient and economical approach to the decomposing of images into multiresolutional representations.[4] Therefore, an orthogonal wavelet (the four coefficient Daubechies wavelet) is used in this research.

Traditionally, image transform coding or compression methods, such as the discrete cosine transform, rely on high energy compaction with an $n \times n$ passband coefficient selection criterion. The wavelet transform generally results in poor energy compaction, so an alternative strategy is required for wavelet coefficient

selection. This paper investigates a multiagent stochastic optimization approach for wavelet coefficient selection, and a statistical derivation of a deterministic equation for wavelet coefficient selection. This derivation is based on empirical data derived from the stochastic optimization of the coefficient thresholds.

1.1. Multiresolution coding theory

Performing the Fourier transform decomposes an image into a frequency representation and allows an analyst to determine if a particular frequency is present, but does not provide any spatial information. The wavelet transform, unlike the Fourier transform, produces a spatial-frequency representation that has good localization in both domains.

The wavelet transform filters the data and results in a lowpass, or blurred, version of the original, and a highpass, or detailed, version. The lowpass image is recursively filtered to produce a blurred and detail image of itself. Because the wavelet transform used in this work is separable, the image wavelet transform can be implemented as successive one-dimensional transforms of the row and columns. The resulting image has a horizontal detailed image, a vertical detailed image, a diagonal detailed image, and a blurred image. Each transform consists of a wavelet dilation. or wavelet resolution.

We are interested in a discrete sublattice of the continuous wavelet since image data is discrete in nature. Thus, the discrete wavelet is

$$\psi_{m,n}(x) = a_0^{-m/2}\psi\left(\frac{x - nb_0a_0^m}{a_0^m}\right) \tag{5}$$

where a_0 and b_0 are constants. In our case, $a_0 = 2$ and $b_0 = 1$. Rewriting the wavelet transform in terms of the inner products of the finer resolution wavelet transform shows that the discrete multiresolutional decomposition can be performed using the filters h and g, given that

$$\begin{aligned} H(0) &= 1 \\ |H(\omega)|^2 + |H(\omega+\pi)|^2 &= 1 \end{aligned} \tag{6}$$

where $H(\omega)$ represents the Fourier transform of the filter h.[5,6] The corresponding highpass filter g is defined via

$$G(\omega) = e^{-j\omega}H^*(\omega+\pi) \tag{7}$$

where $H^*(\cdot)$ is the complex conjugate of $H(\cdot)$, and $G(\omega)$ is the Fourier transform of g.

Directly implementing the wavelet transform as given in Eq. 2 is inefficient. A multiresolutional decomposition algorithm has been developed that accomplishes the wavelet transform in order $N \log N$ operations where N is the length of the data.[7] The algorithm introduces an auxiliary function $\phi(x)$ related to $\psi(x)$ by

$$\psi(x) = \sum_k h(k)\phi(x-k) \tag{8}$$

where $\phi(x)$ satisfies

$$\phi(x) = \sum_k g(k)\phi(2x-k). \tag{9}$$

1.2. Wavelet compression techniques

Wavelet image coding techniques include wavelet[8] and coefficient[9] selection approaches, as well as hybrid schemes which combine wavelets with other signal representations.[10] In a coefficient selection approach, image compression is achieved by retaining a subset of coefficients from the wavelet representation, and zeroing the remaining coefficients. The number of coefficients selected is based on the maximum mean-squared error (MSE) acceptable, the compression ratio required, or a combination of both. The coefficients selected are then coded using an entropy-based encoder that stores the value of the coefficient and its location within the current scale.

Different sets of retained coefficients can result in drastically different image reconstructions. The traditional method for selection is simply a passband filter of some height and width that passes a rectangular region of the transformed data and sets the rest to zero. DeVore et al.[11] show that the wavelet transform does not compact energy into a particular region, making the passband approach suboptimal. DeVore presents a wavelet coefficient selection algorithm that keeps the highest N coefficients and discards the rest. Argast et al.[12] demonstrate that coefficients from lower resolution scales affect a larger part of the image than coefficients in the high resolution scales. Argast presents an algorithm for selecting coefficients based on a logarithmic threshold, where the threshold of each scale is twice the threshold of the previous lower resolution scale. This compression strategy of Argast is given as:

for $J = S$ *to* 1 {
    for each element k *in scale* J
    if $CR\% = GOAL$ *then stop*
    else

$$set\ c_k = \begin{cases} 0 & if\ |c_k| < A \cdot 2^J \\ c_k & otherwise \end{cases}$$

} *end*

where c_k is a transform coefficient, $CR\%$ is the current compression percentage, A is a constant weight factor, and J and S are respectively the current and total wavelet scales. The constant A is set (initially set to 0.01 in their paper) and then iteratively adjusted so that the compression ratio can be met. For a selected compression ratio, this approach results in a lower mean-squared error in the reconstructed images than DeVore's algorithm.

Previous preliminary work[9] has demonstrated an interscale relationship between an image's stochastically derived wavelet coefficient thresholds. This paper increases the number of images stochastically optimized, and for a selected compression ratio, statistically derives from empirical results a deterministic approach for wavelet coefficient selection.

2. STOCHASTIC OPTIMIZATION

Since the 1950's, random (or stochastic) search techniques have been used for function optimization. Random search strategies are competitive with traditional search strategies (such as gradient search techniques) when the cost or objective function is expensive or difficult to compute, or when the function to be minimized has many suboptimal solutions (local minima). Other advantages include the ease of programming, inexpensive realization of possible solutions, as well as flexibility in the expression of the criterion function.[13]

Stochastic optimization techniques are based on either a single point or multiple agent algorithms. Single point algorithms include the random walk, the creeping random method,[14] and the method of Solis and Wets.[15] Multiple agent stochastic search algorithms, such as genetic algorithms,[16] evolutionary strategies,[17] and evolutionary programming (EP),[18] are becoming well known for their optimization properties. A thorough discussion of the EP algorithm, and other evolutionary algorithms, is given by Bäck and Schwefel.[17]

In EP, a population of models (solutions) generate new models via a mutation process. The new models compete with the original (parent) population for survival to the next iteration. The mutation process is a random perturbation of the parameters, with the magnitude of the perturbation generally tied to the fitness of the parent. Although useful in escaping local minima, the random nature of the stochastic mutation process can be inefficient. To increase convergence efficiency, variants of the EP algorithm have been developed.[19,20] The presented work imbeds the method of Solis and Wets into the traditional evolutionary programming paradigm. The parent models not only produce a single offspring by way of the mutation process, but are also modified via the Solis and Wets algorithm. Figure 1 illustrates this hybrid optimization approach.

component corresponds to the final low-pass (DC) component of the wavelet transform). Figure 2 displays a multiresolutional wavelet transform, and the threshold array indices corresponding to the wavelet transform scales.

Figure 2. Multiresolutional wavelet transform and associated scales.

For each image, the compression ratio was set to 50:1 ($CA\% = 2.0\%$). The four coefficient Daubechies wavelet is used for the compression process. Since we are currently interested in the coefficient thresholds, optimization of the wavelet is beyond the scope of this paper. Figure 3 displays the MSE and percentage of selected coefficients of the best coefficient threshold strategy for two images during the stochastic optimization process. As shown in the figures, the best solution of the evolutionary programming process quickly achieves the desired compression ratio.

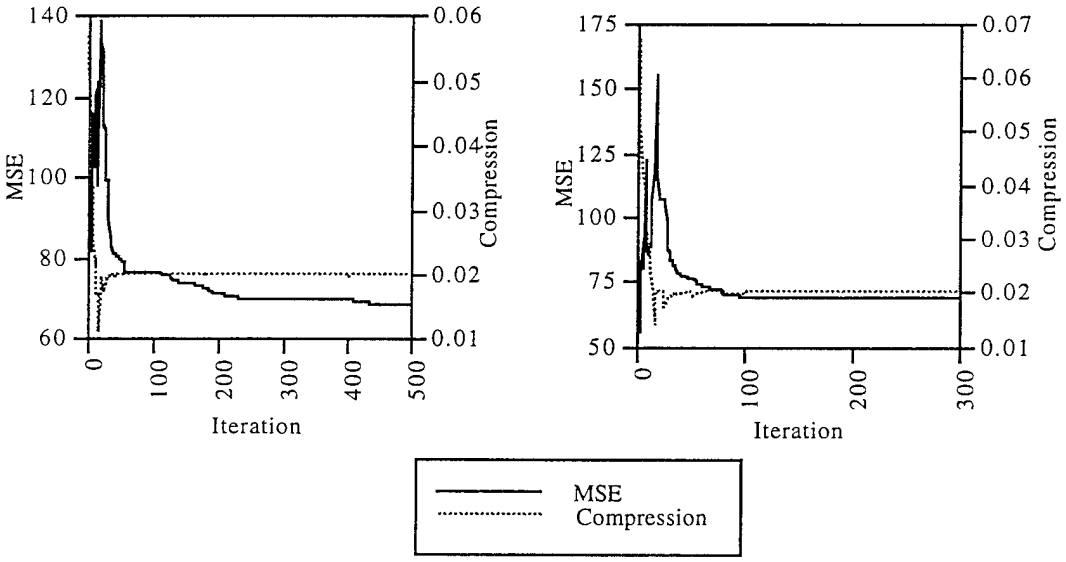

Figure 3. Stochastic optimization performance for two images.

For all of the images compressed, the coefficient threshold values of the best compression strategy (the best T vector) derived after 600 iterations are tabulated in Table 1. The stochastically derived thresholds for several of these images are also shown in Figure 4. It is important to note that for all images, the values for the lower scales are below all wavelet coefficient values in those scales, and therefore all coefficients in these scales are kept for image reconstruction by the compression strategy. Table 1 italicizes the threshold values which are less than the minimum wavelet coefficient value in the respective scale. As shown in the table and figure, the higher scale thresholds generally demonstrate an interscale relationship, with the value of the higher scale roughly double the value of the lower.

Table 1. Derived wavelet coefficient thresholds (*italicized* thresholds < min. scale coefficient value).

Image	0	1	2	3	4	5	6	7	8	9
ape	*2.4653*	*0.7767*	*0*	*0*	*0*	0.6890	1.8321	3.3578	6.7787	7.9643
bird	*9.1476*	*0.7630*	*1.0689*	*0*	0.3163	0.9366	1.7169	3.6900	8.0887	14.233
fruits	*5.8495*	*3.4984*	*3.2286*	*0*	0.4316	1.3324	3.1653	6.9482	14.338	25.711
Lenna	*16.654*	*1.5507*	1.1368	*0*	0.6856	1.6835	3.4750	6.6345	15.244	23.488
light	*21.811*	*6.7336*	*0*	*0*	1.0330	2.3785	5.0125	9.1587	18.91	26.69
ritchie	*7.1629*	*6.9475*	*0*	*0*	0.2866	0.8181	2.2308	4.3514	7.8771	13.065
truck	*0.7322*	*0*	*0.4224*	*0*	1.1629	2.1504	3.6688	5.7335	10.454	19.302
watch	*1.7094*	*0*	*0.2452*	*0*	0.5691	1.5518	2.1343	4.8156	9.9992	15.582
woman1	*34.656*	*0*	*0*	*0*	*0*	1.5520	2.9408	7.0446	13.218	249.16
woman2	*6.3236*	*1.9193*	*0.3891*	*0*	*0*	0.4538	2.0579	3.4584	8.0179	11.838

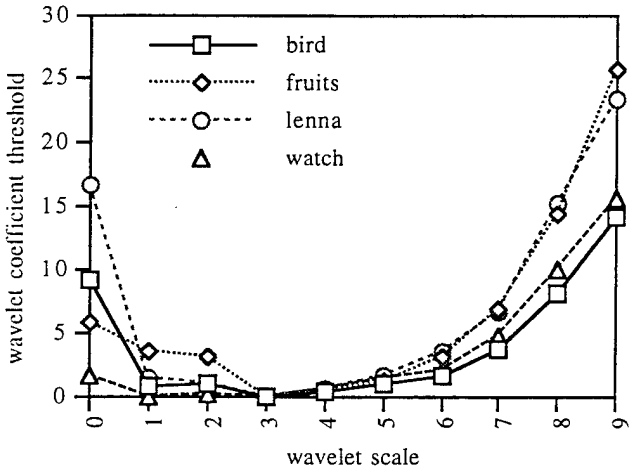

Figure 4. Wavelet coefficient thresholds for several images.

To measure if the coefficient threshold values derived from the optimization process are related to the variance or power* of an image, the intensity histogram of the "watch" image was manipulated and the resulting new images where stored. The coefficient thresholds for each version were stochastically optimized, and the resulting thresholds are displayed in Table 2 and Figure 5. The amount of energy and power of each image were also calculated, and each image's associated power is used to label the images. The figure and table demonstrate that the thresholds are functionally related (in some way) to the energy or power of the image, with images with a higher power content requiring higher coefficient thresholds for efficient image compression.

Table 2. Thresholds for watch image versions (*italicized* thresholds < min. coefficient value).

Power	0	1	2	3	4	5	6	7	8	9
487.681	*1.7094*	*0*	*0.2452*	*0*	0.5691	1.5518	2.1343	4.8156	9.9992	15.582
2463.08	*24.689*	*0*	*0.0633*	0.5338	1.1229	2.0076	5.2575	8.6799	22.546	41.290
3631.97	*5.9185*	*0*	*0*	*0*	1.1298	3.3120	6.6504	12.405	26.771	50.148
809.566	*3.4421*	*0.6452*	*0*	*0*	0.8541	1.3262	3.2021	4.5852	13.538	23.507
6085.99	*6.0353*	*1.0274*	*0*	*0*	1.8211	3.9013	7.8937	16.265	33.507	59.317
1796.08	*6.4429*	*0*	*0.7791*	*0*	1.3001	2.2102	4.8936	8.5007	17.988	33.006
1916.7	*4.3556*	*0*	*0.3967*	*0*	1.0643	2.0814	4.9868	8.8207	18.572	33.955

* The variance or power of an image is defined as $\hat{\sigma}^2 = \frac{1}{N_i N_j} \sum_{ij} (I(ij) - \mu_I)^2$, where $I(ij)$ is the pixel intensity at location (i, j) and μ_I is the mean intensity value of the image.

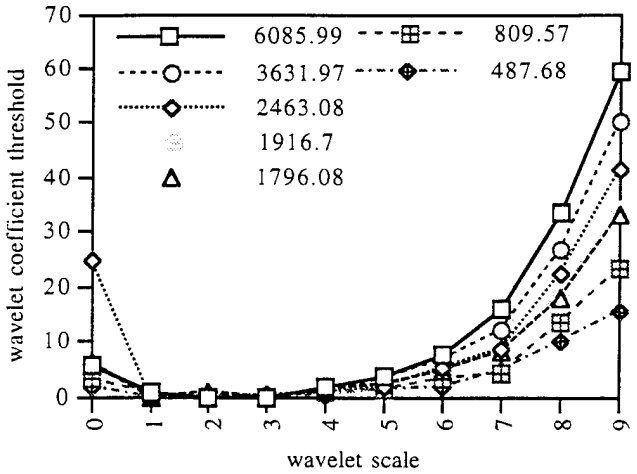

Figure 5. Coefficient thresholds for an image at various levels of power.

5. STATISTICAL ANALYSIS OF HYPOTHESIZED COMPRESSION SCHEME

In this section, we hypothesize the nature of the relationship suggested by the results of the multiagent stochastic optimization process, and derive a deterministic equation based on the statistics derived from the data. For a given compression ratio, we propose a coefficient selection criterion of the form

$$T_i = K(CR) \cdot f(\hat{\sigma}^2) \cdot 2^i \tag{12}$$

where T_i is again the coefficient threshold associated with the ith wavelet scale, $K(CR)$ is a function of the compression ratio, and $f(\hat{\sigma}^2)$ is a function of the power content of the image. In this work, we hypothesize the functional form of $f(\hat{\sigma}^2)$ to be

$$f(\hat{\sigma}^2) = (\hat{\sigma}^2)^B \tag{13}$$

where B is a constant. In this investigation, a single compression ratio has been applied to all images, and therefore K is considered a constant. The hypothesized equation can be written as

$$T_i = K(\hat{\sigma}^2)^B 2^i \tag{14}$$

We will now apply regression analysis techniques to calculate a value for B based on the thresholds derived in the stochastic optimization process. For both constants B and K, only the coefficient thresholds from scales four and above, which actually zero coefficients in the scale, are used for the statistical derivation. Threshold values in scales zero through three are not used in the analysis, since any threshold value below the minimum coefficient value of a scale (i.e. any value T_i such that $0 \le T_i \le \min\{|c_{k,i}|\}$) results in the same image reconstruction.

5.1. Determination of the relationship between threshold value and power

The intensity-adjusted "watch" images, and the stochastically derived coefficient thresholds, are used to determine the relationship between image power and the threshold values. Dividing both sides of Eq. 14 by 2^i and taking the logarithm of both sides gives

$$\log\left(\frac{T_i}{2^i}\right) = B\log(\hat{\sigma}^2) + \log K. \tag{15}$$

This is a linear equation $y = Bx + c$, with $y = \log\left(\frac{T_i}{2^i}\right)$, $x = \log(\hat{\sigma}^2)$, and $c = \log K$, and linear regression techniques[21] are applied for the estimate of B. Given the assumption that the are samples are independent and normally distributed about the true values also allows for statistical inference and validation tests to be performed. The maximum likelihood regression estimate of B is given as

$$\hat{B} = \frac{\sum_{i=1}^{n}(x_i - \bar{x})(y_i - \bar{y})}{\sum_{i=1}^{n}(x_i - \bar{x})^2} \tag{16}$$

Figure 6 displays the sample pairs $y = \log\left(\frac{T_i}{2^i}\right)$ vs. $x = \log(P)$, and line determined by the linear regression estimates for the threshold coefficients under analysis.

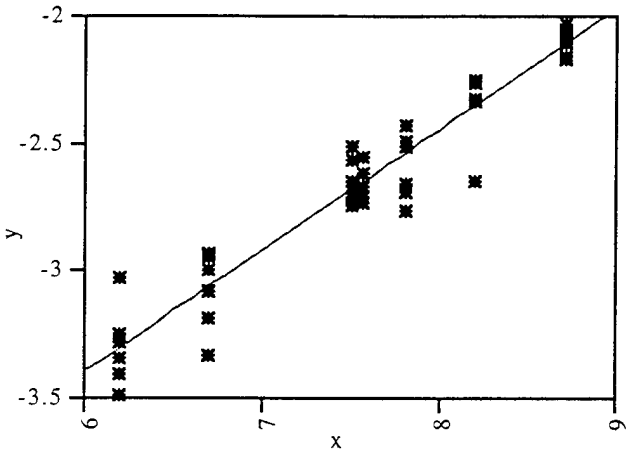

Figure 6. Relationship between and $y = \log\left(\frac{T_i}{2^i}\right)$ and $x = \log(\hat{\sigma}^2)$.

The maximum likelihood value for the slope is computed to be $\hat{B} = 0.4714$, with an associated coefficient of determination for the regression line is equal to $R^2 = 91.37\%$. The value of $\hat{B}$ is very close to 0.5, and assuming the normal model allows the use of the F-statistic associated with the hypothesis that $H_0: B = ½$ vs. $H_1: B \neq ½$. Computing an $\alpha = 0.10$ level of significance test, the corresponding F-statistic requires one to reject $H_0: B = ½$ if the statistic is greater than $F_y(1, 40) = 2.84$. The F-statistic is given as

$$\frac{\left(B_0 - \hat{B}\right)^2}{S^2 / S_{xx}} = \frac{(0.5 - 0.4714)^2}{0.0139 / 26.505} = 1.560 \tag{17}$$

which is less than $F_y(1, 40)$. So one fails to reject that $H_0: B = ½$ based on the data analyzed. This reduces the functional from of Eq. 13 to

$$f(\hat{\sigma}^2) = \hat{\sigma}. \tag{18}$$

Since $B = 0.5$ provides a simple interpretation, with coefficient threshold values directly related to the standard deviation of the image intensities, we will use $B = 0.5$ for the determination of the constant K.

5.2. Determination of the constant K

Given the derived value of B, our hypothesized equation (Eq. 14) is now

$$T_i = K\hat{\sigma}2^i \tag{19}$$

Dividing both sides by $\hat{\sigma}2^i$ derives a value of K_i for each image and scale under analysis, and these values are used as a sample to derive an estimate of K. Nine images of Table 1 are used for the computation of K, with the "Lenna" image reserved for algorithm testing and comparison. It was found that the mean value of K did not achieve adequate compression on the test image, since the mean will "on average" produce the desired compression. To more adequately achieve the desired compression ratio, one-half of a standard deviation of the $\{K_i\}$ sample is added to the mean $\overline{K}$ to produce K. K is simply computed as

$$K = \overline{K} + \frac{s_k}{2} \tag{20}$$

Note that the highest scale threshold value of image "woman2" is a wild point, and this value was not used in the computation of $\overline{K}$. For the images analyzed, the estimate $\overline{K}$ is computed as $\overline{K} = 9.360 \cdot 10^{-4}$, and the standard deviation of $\{K_i\}$ is $s_k = 6.217 \cdot 10^{-4}$. The median of the $\{K_i\}$ sample, a more robust measure of centrality when wild points exist, is in close agreement with $\overline{K}$, with $K_{MED} = 9.604 \cdot 10^{-4}$. For the single compression ratio (50:1) examined in this paper, our hypothesized deterministic equation is finalized as

$$T_i = \left(1.247 \cdot 10^{-3} \cdot \hat{\sigma}\right) 2^i. \tag{21}$$

Unlike the algorithms of DeVore and Argast and the stochastically optimization approach, the coefficients of Eq. 21 have been statistically determined, and the resulting compression ratio for an image using Eq. 21 will not be exactly 50:1. However, this equation requires neither coefficient sorting nor iterative optimization, and is therefore computationally more efficient than the other approaches. The next section compares this deterministic equation with the algorithms previously discussed in Section 2 on the "Lenna" image.

6. COMPARISON OF IMAGE COMPRESSION APPROACHES

The "Lenna" image, not used for the statistical determination of Eq. 21, is used for a comparative analysis of the wavelet compression algorithms. Table 3 compares the algorithms of DeVore, Argast, the stochastically determined thresholds, and the wavelet coefficient thresholds calculated using the deterministic equation (Eq. 21), on the "Lenna" image.

Table 3. Comparison of algorithms on the "Lenna" image.

Algorithm	MSE	% of Distortion	Signal-to-Noise	Compression Ratio
DeVore	135.24	5.91 %	12.29 dB	50:1
Argast	75.80	3.31 %	14.80 dB	50:1
Stochastic	68.26	3.02 %	15.19 dB	50:1
Eq. 21	75.87	3.31 %	14.80 dB	56:1

Unfortunately, the standard deviation of the sample $\{K_i\}$ is on the same order of magnitude as the mean $\overline{K}$, and this indicates that the estimates of K vary dramatically in the sample. This variability is illustrated in Table 4, where the MSE and achieved compression ratio are compared for four images. As shown in the table, the compression ratio for the equation ranges from 33:1 to 86:1. This is due to the large deviation of the estimates for K in the images analyzed. This variability severely limits the usefulness of the deterministic equation when achievement of a compression ratio is required, and brings the assumption that K is a function of compression ratio into question.

Table 4. Comparison of algorithm MSE and compression ratio on four images.

Image	light		bird		fruits		truck	
Algorithm	MSE	CR	MSE	CR	MSE	CR	MSE	CR
DeVore	193.91	50:1	30.73	50:1	141.87	50:1	124.04	50:1
Argast	129.38	50:1	19.81	50:1	80.13	50:1	80.74	50:1
Stochastic	118.15	50:1	19.50	50:1	68.97	50:1	75.40	50:1
Eq. 21	152.28	66:1	34.30	86:1	83.68	64:1	58.26	33:1

As shown by Tables 3 and 4, the wavelet coefficient thresholds found by the stochastic optimization process are superior to all other approaches discussed in this work. For every image tested, the multiagent stochastic process produced the coefficient threshold strategy with the minimum MSE. The method of Argast, although outperformed by our stochastic optimization process, was significantly better than the method of DeVore for all images tested.

Figure 7 displays the original and restored "Lenna" images. These images represent the results from the application of the various 50:1 wavelet compression approaches, each using the four-coefficient wavelet of Daubechies.

7. CONCLUSIONS

In conclusion, multiagent stochastic optimization provides a valuable tool for the investigation of complex problems. In this work, we have developed a stochastic optimization technique to determine the wavelet coefficient thresholds which best compress and restore an image for a given compression ratio. With the stochastically-derived wavelet coefficient thresholds, we have shown evidence of a strong statistical relationship between threshold magnitude and the power of the image. For every image analyzed and tested, the compression strategy derived via our stochastic optimization process outperforms the iterative and sorting wavelet coefficient threshold procedures, producing compression strategies that achieve the required compression with the consistently minimal MSE.

A deterministic threshold selection equation, based on the stochastically-derived thresholds, was derived. This equation has shown superior capability for image reconstructive ability when compared to the approach of DeVore, and is computationally more efficient than the techniques of Argast or Waagen et al.[9] However, the variability of the hypothesized constant K limits the equation's usefulness for image compression to situations with "on-average" compression requirements.

This work represents ongoing research, and future work will investigate the functional relationship between wavelet coefficient threshold values and the desired compression ratio for several compression ratios. Other criteria for image compression include optimization based on a desired MSE, or distortion percentage, will also be investigated. The hypothesized equation for image compression will be re-evaluated, with the goal of minimizing the variability of any constants in the equation. The sensitivity of the threshold selection equation to the formulation of the wavelet function is also a valuable topic for research.

8. REFERENCES

1. J. Morlet, G. Arens, E. Fourgeau, and D. Giard, "Wave propagation and sampling theory," *Geophysics*, Vol. 47, pp. 203-236, 1982.
2. I. Daubechies, *Ten Lectures on Wavelets*, SIAM, Philadelphia, 1992.
3. Y. Meyer, *Wavelets: Algorithms & Applications*, SIAM, Philadelphia, 1993.
4. O. Rioul, "A discrete-time multiresolution theory," *IEEE Transactions on Signal Processing*, Vol. 41 No. 8, pp. 2591-2606, 1993.
5. I. Daubechies, "Orthonormal bases of compactly supported wavelets," *Comm. of Pure and Applied Mathematics*, Vol. 41, pp. 909-996, 1988.
6. G. Strang, "Wavelets and dilation equations: A brief introduction," *SIAM Review*, Vol. 31 No. 4, pp. 614-627, 1989.
7. S. Mallat, "A theory for multiresolutional signal decomposition: The wavelet representation", *IEEE Transactions on Pattern Recognition and Machine Intelligence*, Vol. 11 No. 7, pp. 674-693, 1989.
8. A. H. Tewfik, D. Sinha, and P. Jorgensen, "On the optimal choice of a wavelet for signal representation," *IEEE Transactions on Information Theory*, Vol. 38 No. 2, pp. 747-765, 1992.
9. D. E. Waagen, J. D. Argast, and J. R. McDonnell, "Evolving wavelet compression strategies," *Third Annual Conference on Evolutionary Programming*, San Diego, 1994.
10. A. C. Ansari, I. Gertner, and Y. Y. Zeevi, "Combined wavelets-DCT image compression," *Signal Processing, Sensor Fusion, and Target Recognition*, Vol. 1699, pp. 308-316, SPIE, Orlando, 1992.
11. R. A. DeVore, B. Jawerth, and B. J. Lucier, "Image compression through wavelet transform coding," *IEEE Transactions on Information Theory*, Vol. 38 No. 2, pp. 719-746, 1992.
12. J. Argast, M. Rampton, X. Qiu, and T. Moon, "Image compression with the wavelet transform," *Visual Communication and Image Processing*, Vol. 2094, 1993.
13. D. C. Karnopp, "Random search techniques for optimization problems," *Automatica*, Vol. 1, pp. 111-121, 1963.
14. S. H. Brooks, "A discussion of random methods for seeking maxima," *Operations Research*, Vol. 6, pp. 244-251, 1958.

15. F. J. Solis and R. J. B. Wets, "Minimization by random search techniques," *Mathematics of Operations Research*, Vol. 6 No. 1, pp. 19-30, 1981.
16. D. Goldberg, *Genetic Algorithms in Search Optimization and Machine Learning*, Addison-Wesley, Reading, 1989.
17. T. Bäck and H. P. Schwefel, "An overview of evolutionary algorithms for parameter optimization," *Evolutionary Computation*, Vol. 1 No. 1, pp. 1-23, 1993.
18. D. B. Fogel, *Evolving Artificial Intelligence*, Ph.D. dissertation, University of California, San Diego, 1992.
19. D. E. Waagen, J. R. McDonnell, and P. Diercks, "The stochastic direction-set algorithm: a hybrid technique for finding function extrema," *First Annual Conference on Evolutionary Programming*, pp. 35-42, San Diego, 1992.
20. J. R. McDonnell and D. E. Waagen, "Evolving recurrent perceptrons for time-series modeling," *IEEE Transactions on Neural Networks*, Vol. 5 No. 1, pp. 24-38, 1994.
21. G. Cassella and R. L. Berger, *Statistical Inference*, Brooks/Cole, Belmont, 1990.

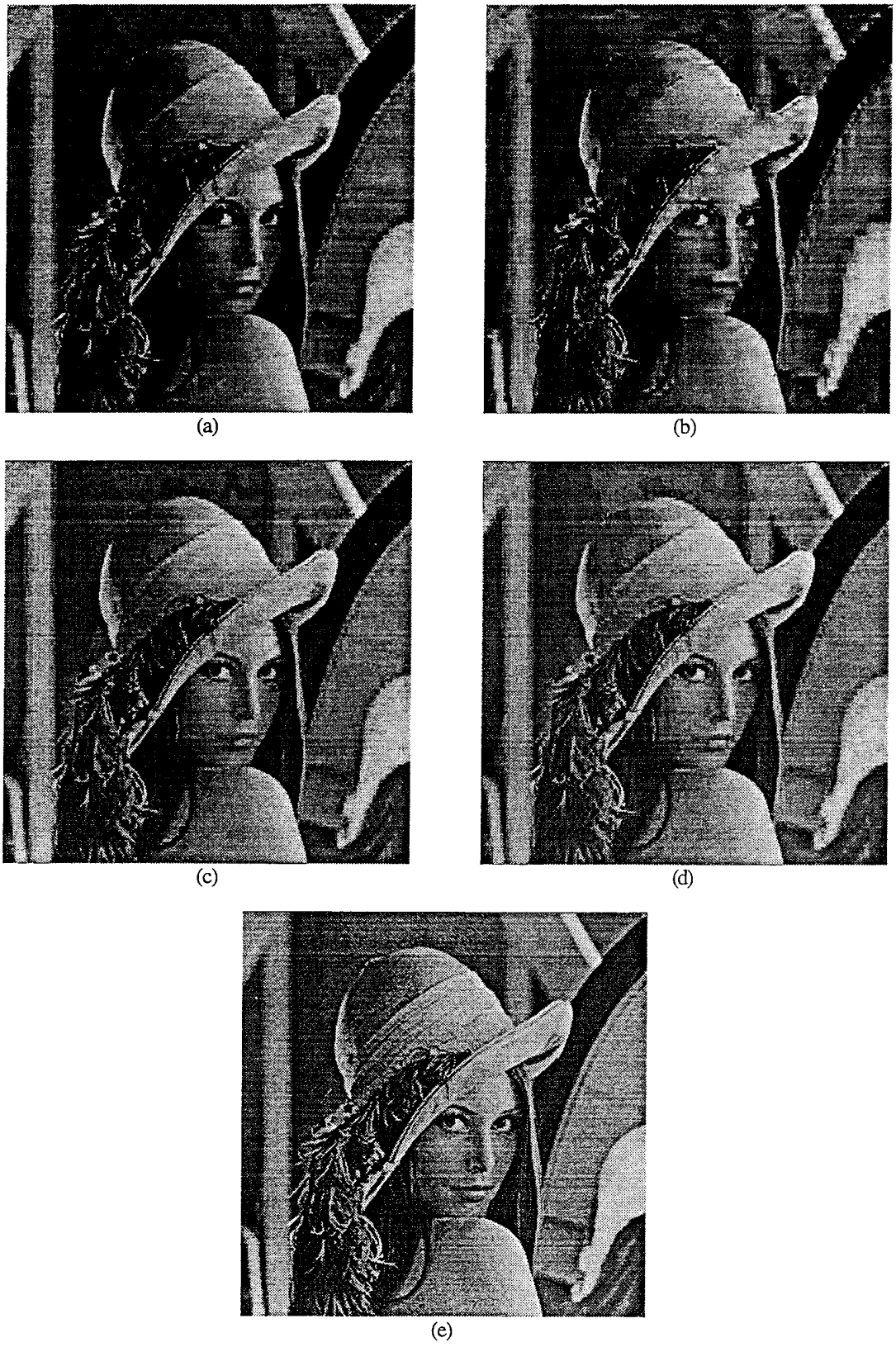

Figure 7. Image reconstructions from 50:1 compressed representations generated by Argast (a), DeVore (b), stochastic optimization (c), and Eq. 21 (d) (at 56:1) approaches. Original image (e).